Effects of Anthropogenic Forcing and Natural Variability on the 2018 Heatwave in Northeast Asia

YITIAN QIAN, HIROYUKI MURAKAMI, PANG-CHI HSU, AND SARAH B. KAPNICK

AFFILIATIONS:

QIAN —*Key Laboratory of Meteorological Disaster of Ministry of Education, Nanjing University of Information Science and Technology, China, and National Oceanic and Atmospheric Administration/Geophysical Fluid Dynamics Laboratory, and Atmospheric and Oceanic Sciences Program, Princeton University, Princeton, New Jersey;*

MURAKAMI—*National Oceanic and Atmospheric Administration/Geophysical Fluid Dynamics Laboratory, Princeton, New Jersey, and University Corporation for Atmospheric Research, Boulder, Colorado;*

HSU—*Key Laboratory of Meteorological Disaster of Ministry of Education, Nanjing University of Information Science and Technology, China;*

KAPNICK—*National Oceanic and Atmospheric Administration/Geophysical Fluid Dynamics Laboratory, Princeton, New Jersey*

CORRESPONDING AUTHOR: Hiroyuki Murakami, hir.murakami@gmail.com

DOI:10.1175/BAMS-D-19-0156.1

The Northeast Asian 2018 heatwave is an *unlikely* event without anthropogenic forcing; only two have occurred over the last 40 years. By 2050 they will become 1-in-4-yr events.

In the summer (July–August) of 2018 a record-breaking heatwave (HW) spread across Northeast Asia (NEA; 34°–40°N, 120°–143°E; Figs. 1a–c). Maximum 2-m air temperature (T_{max}) anomalies over NEA in that summer were about +1.5°C, more than 1.5 standard deviations above the average using the three reanalysis datasets (Fig. 1d). It was the second highest anomaly since 1980. The subtropical high (Tibetan high) in the middle (upper) troposphere moved northwestward (northeastward) with a positive anomaly over NEA (see Figs. ES1a,1b in the online supplemental material). An equivalent barotropic structure (Figs. ES1a,b,f) characterized by large-scale subsidence emerged, providing a favorable condition for extreme hot days in NEA (JMA 2018).

Several processes might have contributed to the 2018 HW (Enomoto 2004; Zhu et al. 2011; Lee and Lee 2016). Anthropogenic warming has contributed to increasing HW frequency and intensity in recent decades (Song et al. 2015; Sippel et al. 2016; Oliver et al. 2018). Natural variability can also contribute to HWs over Asia. Anomalous cyclonic circulation over the Indo-Pacific warm pool region inducing more active convection (Fig. ES1e) and diabatic heating could induce high temperature anomalies near NEA through exciting a Rossby wave train (Chen and Lu 2014; Lee and Lee 2016). This teleconnection may result from tropical sea surface temperature anomalies (SSTAs) associated with El Niño–Southern Oscillation (ENSO). Previous studies (e.g., Zhu et al. 2007; Wu et al. 2010; Lee and Lee 2016) identified a negative relationship between NEA summer temperature and the Niño-3.4 index (area-averaged SSTA over 5°S–5°N, 170°–120°W). The Arctic Oscillation (AO) can also influence circulation anomalies over NEA via a strong circumpolar vortex (Fig. ES1f), shifting the location of the subtropical jet farther north (Fig. ES1c; Lee and Lee

2016). Matsumura and Horinouchi (2016) found that a negative Pacific decadal oscillation (PDO) phase with a warmer surface condition near NEA (Fig. ES1e) could lead to a positive geopotential height anomaly, which could also be related to NEA HWs. In this study, we address the impacts of anthropogenic forcing and natural variability (i.e., ENSO, PDO, and AO) on the occurrence of the 2018 NEA HW and quantify future projections of NEA HWs using a large ensemble of simulations from a global coupled model developed at the Geophysical Fluid Dynamics Laboratory (GFDL).

Data and methods.

Daily T_{max} is taken from three state-of-the-art reanalysis datasets: ERA-Interim (Dee et al. 2011), MERRA2 (Gelaro et al. 2017), and JRA-55 (Kobayashi et al. 2015). Large-scale atmospheric variables are derived from ERA-Interim. Sea surface temperature (SST) is obtained from HadISST1 (Rayner et al. 2003) and precipitation is obtained from the Global Precipitation Climatology Project (Adler et al. 2003). All datasets are regridded to 1.5° × 1.5°. Observed natural indices (Niño-3.4, PDO, and AO) were downloaded from their official websites (NOAA/ESRL 2019; NOAA 2019; NOAA/CPC 2019). All natural indices are averaged in summer (July–August) and normalized to 1980–2018.

We conduct a suite of simulations using the 50-km-mesh GFDL Forecast-oriented Low Ocean Resolution model (FLOR; Vecchi et al. 2014). We examine two types of multidecadal simulations. One of them is a 35-member multidecadal simulation experiments (AllForc), in which the CMIP5 (phase 5 of the Coupled Model Intercomparison Project) historical natural, anthropogenic, and aerosol forcings up to 2005 are prescribed; future projected levels are based on the CMIP5 RCP4.5 scenario for 2006–50. AllForc is compared with a 30-member 1941 forcing experiments (1941Forc), in which anthropogenic radiative forcing is fixed at the year 1941 value for years 1941–2050; natural forcing varies from year to year in this experiment (Murakami et al. 2015, 2017; Zhang et al. 2017).

We define three HW-related variables in this study. First, we define the T_{max} anomaly (TAnom). Observed and simulated TAnom is defined as the T_{max} anomaly relative to the summer climatology over 1980–2018. Next we define two different heat wave day (HWD) events: modest and extreme. For modest HWD events, the 75th percentile of daily T_{max} for each calendar day during 1 July–31 August with a 15-day window (e.g., 23 June–7 July on 1 July) over 1980–2018 is selected. Thus, 585 samples (15 days × 39 years) for observations and 20,475 samples (15 days × 39 years × 35 members) for AllForc were used. We define a modest HWD event when a daily T_{max} exceeds the 75th percentile for at least seven consecutive days. An extreme HWD event is calculated in the same way, but when T_{max} exceeds the 90th percentile for at least three consecutive days. HWDs are the total number of days that meet each HW criteria in a summer. Note that the simulated T_{max} is calibrated by an inflation method to reduce model bias before computing HW-related variables (Johnson and Bowler 2009; see the supplemental information).

Most of the grids over the NEA region experienced both modest (blue pluses) and extreme (black dots) HWDs for more than 10 days in summer 2018 (Figs. 1a–c). To obtain NEA area-averaged results, the three HW-related variables were first computed on individual grids, and then the area average was taken over the NEA domain. The anomalies of area-averaged extreme and modest HWDs in 2018 were 11.1 and 12.2, respectively; this is

comparable to the year with the most HWDs since 1980: 10.2 and 12.7 days in 1994 (Figs. 1e,f).

To assess the simulation ability of FLOR, the three HW-related variables in AllForc are compared with observations. AllForc can capture the amplitude of observed variability of the three HW-related variables well (Figs. 1d–f). Note that the observations are within the range of the ensemble spreads for all but for a few years, justifying our use of the FLOR model for our analysis.

To evaluate the fraction of attributable HW risk to anthropogenic forcing ($FAR_{AllForc}$; Jaeger et al. 2008), $FAR_{AllForc}$ is defined as $FAR_{AllForc} = 1 - (P_{1941Forc}/P_{AllForc})$, where $P_{AllForc}$ ($P_{1941Forc}$) is the occurrence probability of extreme HW years in AllForc (1941Forc). The occurrence probability of an extreme HW year like 2018 [$P(x)$] in AllForc ($P_{AllForc}$) and 1941Forc ($P_{1941Forc}$) is

$$P(x) = \frac{\text{Numbers of year with VAR} \geq x}{\text{Total numbers of years}},$$

where VAR is a HW-related variable, and $P(x)$ represents the probability of a year with VAR value being no less than x. Because the observed 2018 HW falls into a 95th percentile or higher extreme year during 1980–2018, we choose x at the 95th percentile of all the VAR values from AllForc ensemble during 1980–2018 [i.e., from 1,365 (35 members × 39 years) sampling years]. The same x value is applied to the AllForc and 1941Forc ensembles to compute $P_{AllForc}$ and $P_{1941Forc}$ over each time period: 1941–79, 1980–2018, and 2019–50. A $FAR_{AllForc}$ value close to 1 (ranging from $-\infty$ to 1) implies that the extreme HW year is virtually impossible without an increase in anthropogenic forcing.

Results.

The probability density functions for HW-related variables in AllForc have similar distributions with those of the observations, indicating reasonable simulations of the HW-related variables by FLOR (Figs. 2a–cfig2). The three $FAR_{AllForc}$ values are in the range of 0.75–0.82, indicating that the potential risk of extreme HW years increases with enhanced anthropogenic forcing.

Figures 2d–f compare $P_{AllForc}$ (light gray bars) with $P_{1941Forc}$ (dark gray bars) for each of the present decades (1980–2018), past decades (1941–79), and future decades (2019–50). Compared with the rare occurrence of 0.05 (1.5 times per 30 years) of $P_{AllForc}$ during the present decades, $P_{1941Forc}$ is nearly zero, suggesting significant increase of probability due to anthropogenic forcing. Moreover, $P_{AllForc}$ in future decades is projected to increase substantially: up to 0.24–0.28 (7–8 times per 30 years). This implies that an extreme NEA HW year like 2018 would occur about once every four years in the next three decades.

Potential influences of natural variability (e.g., ENSO, PDO, and AO) are also detected by comparing conditional $P_{AllForc}$ for which $P_{AllForc}$ is separately computed during different phases of natural variability [colored markers in Figs. 2d–f; detailed methods are given in Murakami et al. (2015)]. The potential effects of natural variability on $P_{AllForc}$ are measured by the lengths of the colored lines. The increased conditional $P_{AllForc}$ during both the positive phase of the AO and the negative phases of the ENSO and PDO over the present decades indicates that the positive AO ($+2\sigma$) and negative PDO (-0.4σ) increase the probability of a

HW event. However, the modest El Niño condition (+0.2σ) (Fig. ES2) reduces the likelihood of a HW event. Overall, the effect of natural variability on the occurrence of 2018 HW is not negligible, but appears smaller than that of anthropogenic forcing. However, it is uncertain if FLOR perfectly reproduces the observed relationship between natural variability and HW. This uncertainty reduces our confidence in making clear statements of changes in the influence of natural variability on regional HWs without further research.

Conclusions.

A suite of large ensemble simulations using FLOR allows us to explore the probability of NEA HW events over the period of 1941–2050. We find that anthropogenic climate change increases the probability of the NEA 2018 HW event. Natural variability conditions (negative PDO and positive AO) may have also made the event more likely. Anthropogenic forcing will make extreme HWs (like that in 2018) 5 times more likely in future decades.

Acknowledgments.

The authors thank Dr. Nat Johnson, Dr. Liwei Jia, Dr. Gan Zhang, Dr. Salvatore Pascale, and three anonymous reviewers for their suggestions and comments. This work was partly supported by the National Key R&D Program of China (2018YFC1505804) and the China Scholarship Council (File 201808320271).

REFERENCES

Adler, R. F., and Coauthors, 2003: The version 2 Global Precipitation Climatology Project (GPCP) Monthly Precipitation Analysis (1979–present). *J. Hydrometeor.*, **4**, 1147–1167, https://doi.org/10.1175/1525-7541(2003)004<1147:TVGPCP>2.0.CO;2.

Chen, W., and R. Y. Lu, 2014: The interannual variation in monthly temperature over Northeast China during summer. *Adv. Atmos. Sci.*, **31**, 515–524, https://doi.org/10.1007/s00376-013-3102-3.

Dee, D. P., and Coauthors, 2011: The ERA-Interim reanalysis: Configuration and performance of the data assimilation system. *Quart. J. Roy. Meteor. Soc.*, **137**6, 553–597, https://doi.org/10.1002/qj.828.

Enomoto, T., 2004: Interannual variability of the Bonin high associated with the propagation of Rossby waves along the Asian jet. *J. Meteor. Soc. Japan*, **82**, 1019–1034, https://doi.org/10.2151/jmsj.2004.1019.

Gelaro, R., and Coauthors, 2017: The Modern-Era Retrospective Analysis for Research and Applications, version 2 (MERRA-2). *J. Climate*, **30**4, 5419–5454, https://doi.org/10.1175/JCLI-D-16-0758.1.

Jaeger, C. C., J. Krause, A. Haas, R. Klein, and K. Hasselmann, 2008: A method for computing the fraction of attributable risk related to climate damages. *Risk Anal.*, **28**, 815–823, https://doi.org/10.1111/j.1539-6924.2008.01070.x.

JMA, 2018: xxxx. Japan Meteorological Agency, 21 pp., https://www.jma.go.jp/jma/press/1808/10c/h30goukouon20180810.pdf.

Johnson, C., and N. Bowler, 2009: On the reliability and calibration of ensemble forecasts. *Mon. Wea. Rev.*, **137**, 1717–1720, https://doi.org/10.1175/2009MWR2715.1.

Kobayashi, S. Y., and Coauthors, 2015: The JRA-55 reanalysis: General specifications and basic characteristics. *J. Meteor. Soc. Japan*, **93**, 5–48, https://doi.org/10.2151/jmsj.2015-001.

Lee, W.-S., and M. I. Lee, 2016: Interannual variability of heat waves in South Korea and their connection with large-scale atmospheric circulation patterns. *Int. J. Climatol.*, **36**5, 4815–4830, https://doi.org/10.1002/joc.4671.

Matsumura, S., and T. Horinouchi, 2016: Pacific Ocean decadal forcing of long-term changes in the western Pacific subtropical high. *Sci. Rep.*, **6**, 37765, https://doi.org/10.1038/srep37765.

i.s7.*e***0** 4-1>Murakami, H., G. A. Vecchi, T. L. Delworth, K. Paffendorf, L. Jia, R. Gudgel, and F. Zeng, 2015: Investigating the influence of anthropogenic forcing and natural variability on the 2014 Hawaiian hurricane season [in "Explaining Extreme Events of 2014 from a Climate Perspective"]. *Bull. Amer. Meteor. Soc.*, **96**2 (12), S115–S119, ehttps://doi.org/10.1175/BAMS-D-15-00119.1.

Murakami, H., and Coauthors, 2017: Dominant role of subtropical Pacific warming in extreme eastern Pacific hurricane seasons: 2015 and the future. *J. Climate*, **30**, 243–264, https://doi.org/10.1175/JCLI-D-16-0424.1.

NOAA, 2019: PDO index, accessed xxx, https://www.ncdc.noaa.gov/teleconnections/pdo/.

NOAA/CPC, 2019: AO Index, accessed xxx, https://www.cpc.ncep.noaa.gov/products/precip/CWlink/daily_ao_index/monthly.ao.index.b50.current.ascii.

NOAA/ESRL, 2019: Niño-3.4 index, accessed xxxx, https://www.esrl.noaa.gov/psd/gcos_wgsp/Timeseries/Nino34/.

Oliver, E. C. J., S. E. Perkins-Kirkpatric, N. J. Holbrook, and N. L. Bindoff, 2018: Anthropogenic and natural influences on record 2016 marine heat waves [in "Explaining Extreme Events of 2016 from a Climate Perspective"]. *Bull. Amer. Meteor. Soc.*, **99** (1), S44–S48, https://doi.org/10.1175/BAMS-D-17-0093.1.

Rayner, N. A., D. E. Parker, E. B. Horton, C. K. Folland, L. V. Alexander, D. P. Rowell, E. C. Kent, and A. Kaplans, 2003: Global analyses of sea surface temperature, sea ice, and night marine air temperature since the late nineteenth century. *J. Geophys. Res.*, **108**4, 4407, https://doi.org/10.1029/2002JD002670.

Sippel, S., F. E. L. Otto, M. Flach, and G. J. van Oldenborgh, 2016: The role of anthropogenic warming in 2015 central European heat waves [in "Explaining Extreme Events of 2015 from a Climate Perspective"]. *Amer. Meteor. Soc.*, **97** (12), S51–S56, https://doi.org/10.1175/BAMS-D-16-0150.1.

Song, L., S. Dong, Y. Sun, G. Ren, B. Zhou, and P. A. Stott, 2015: Role of anthropogenic forcing in 2014 hot spring in northern China [in "Explaining Extreme Events of 2014 from a Climate Perspective"]. *Amer. Meteor. Soc.*, **96** (12), S111–S114, https://doi.org/10.1175/BAMS-D-15-00111.1.

Vecchi, G. A., and Coauthors, 2014: On the seasonal forecasting of regional tropical cyclone activity. *J. Climate*, **27**1, 7994–8016, https://doi.org/10.1175/JCLI-D-14-00158.1.

Wu, R., S. Yang, S. Liu, L. Sun, Y. Lian, and Z. Gao, 2010: Changes in the relationship between Northeast China summer temperature and ENSO. *J. Geophys. Res.*, **115**1, D21007, https://doi.org/10.1029/2010JD014422.

Zhang, W., and Coauthors, 2017: Influences of natural variability and anthropogenic forcing on the extreme 2015 accumulated cyclone energy in the western North Pacific [in "Explaining Extreme Events of 2015 from a Climate Perspective"]. *Bull. Amer. Meteor. Soc.*, **96**, S131–S143, https://doi.org/10.1175/BAMS-D-16-0146.1.

Zhu, Y., X. Yang, X. Chen, S. Zhao, and X. Sun, 2007: Interdecadal variation of the relationship between ENSO and summer interannual climate variability in China. *J. Trop. Meteor.*, **13**, 132–136.

Zhu, Y., H. Wang, W. Zhou, and J. Ma, 2011: Recent changes in the summer precipitation pattern in East China and the background circulation. *Climate Dyn.*, **36**, 1463–1473, https://doi.org/10.1007/s00382-010-0852-92.

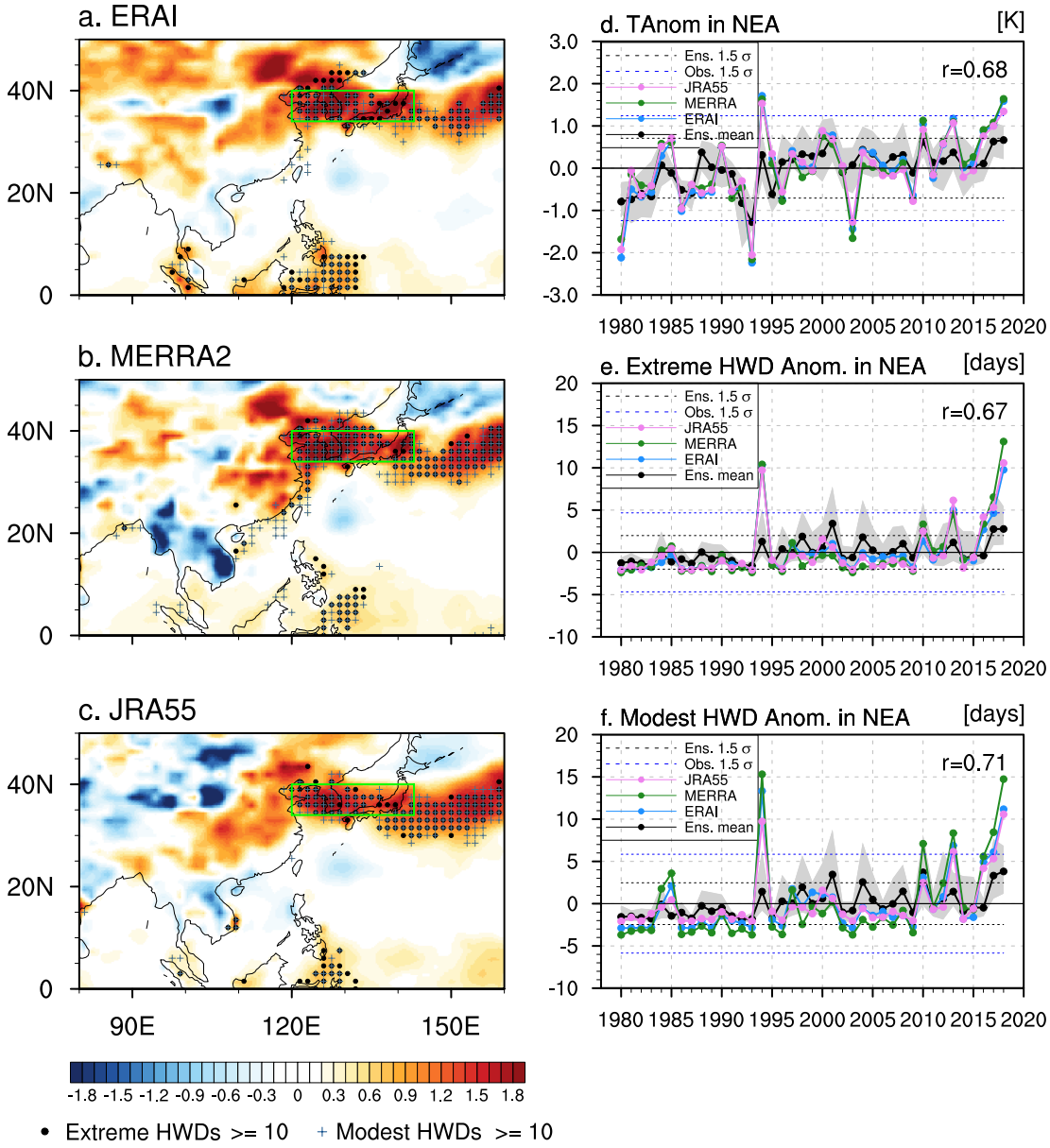

FIG. 1. Daily T_{max} 2018 summer (July–August) anomaly (shading) in (a) ERA-Interim, (b) MERRA2, and (c) JRA55. Black dots (blue pluses) indicate that extreme (modest) HW events occurred for more than 10 days. Interannual variability averaged over NEA (34°–40°N, 120°–143°E; green box in (a)–(c) for (d) daily maximum air temperature anomaly (K), (e) extreme HWD anomaly (days), and (f) modest HWD anomaly (days). Black lines denote individual ensemble members of AllForc (35 total). Blue lines denote the average of three reanalysis datasets (ERA-Interim, MERRA2, and JRA-55). Shadings represent the range from minimum to maximum among the three reanalysis datasets (blue) and 35 ensemble members of AllForc (gray). Blue dashed lines represent ±1.5 standard deviations (σ) of the ensemble mean of the three reanalysis datasets during 1980–2018.

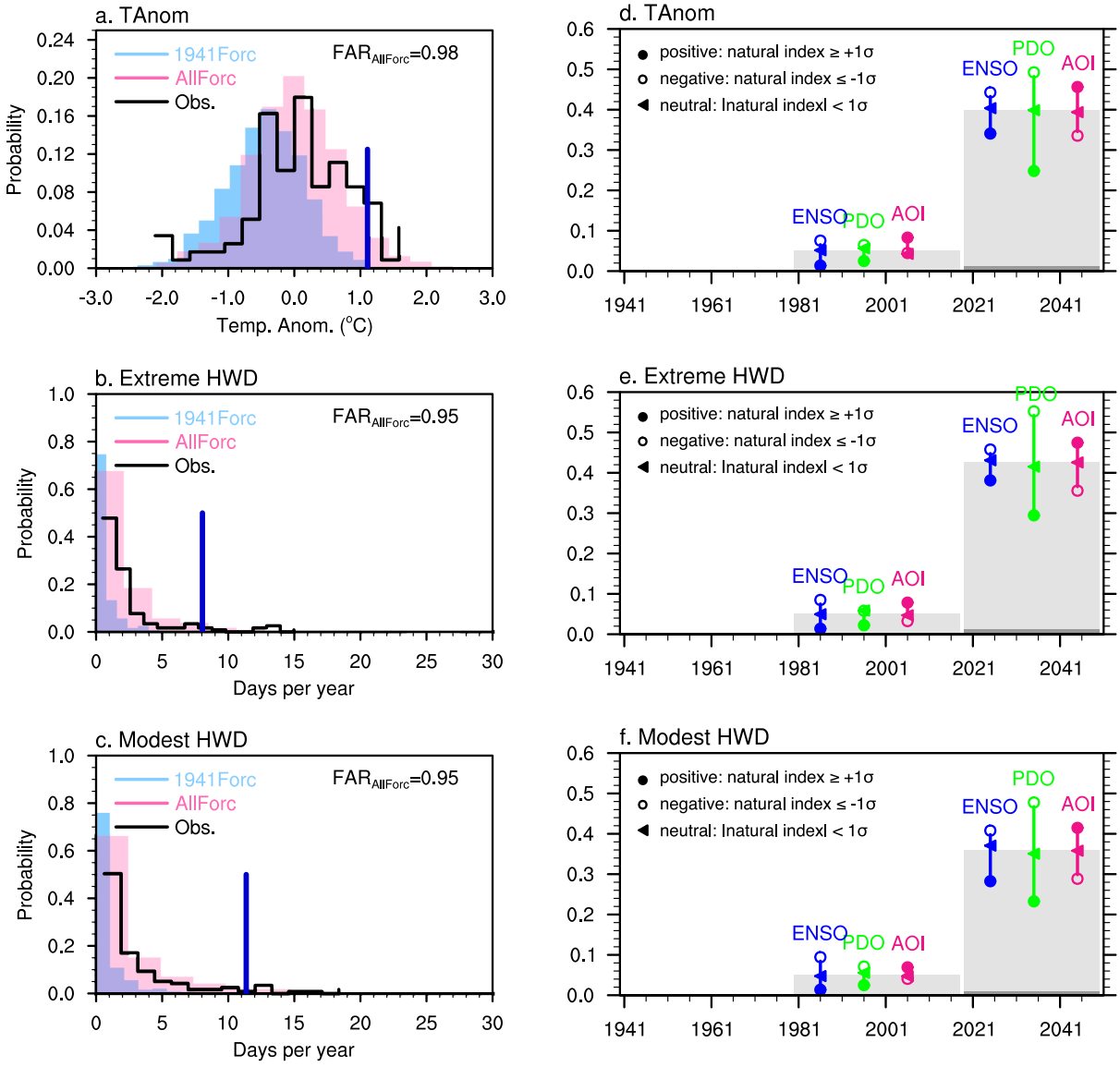

FIG. 2. Probability distribution frequencies of (a) TAnom, (b) extreme HWDs, and (c) modest HWDs based on the three reanalysis datasets (black lines), 1941Forc (sky blue bars), and AllForc (pink bars) during 1980–2018. The thick dark blue lines represent the 95th percentile values in AllForc. $FAR_{AllForc}$ values are shown. Also shown are $P_{AllForc}$ (light gray bars) and $P_{1941Forc}$ (dark gray bars) for (d) TAnom, (e) extreme HWDs, and (f) modest HWDs during the past decades (1941–79), present decades (1980–2018), and future decades (2019–50). The solid (hollow) circles and triangles represent conditional probability of $P_{AllForc}$ during positive (negative) and neutral phases of the ENSO (blue markers), PDO (green markers), and AO (deep pink markers) of present and future decades.